Theoretical upper limits of the thermal conductivity of Si_3N_4

Hao Zhou, Tianli Feng*

Department of Mechanical Engineering, University of Utah, Salt Lake City, Utah 84112, USA

Corresponding Authors

*Email: tianli.feng@utah.edu

Abstract

Silicon nitride (Si_3N_4) is a promising substrate for high-power electronics due to its superior mechanical properties and potential outstanding thermal conductivity (κ). As experiments keep pushing the upper limit of κ of Si_3N_4, it is believed that it can reach 450 W/mK, similar to SiC, based on classical models and molecular dynamics simulations. In this work, we reveal from first principles that the theoretical κ upper limits of β-Si_3N_4 are only 169 and 57 W/mK along the *c* and *a* axes at room temperature, respectively. Those of α-Si_3N_4 are about 116 and 87 W/mK. The predicted temperature-dependent κ matches well with the highest available experimental data, which supports the accuracy of our calculations and suggests that the κ upper limit of Si_3N_4 has already been reached in the experiment. Compared to other promising semiconductors (e.g., SiC, AlN, GaN), Si_3N_4 has a much lower κ than expected even though the chemical bonding and mechanical strengths are close or even stronger. We find the underlying reason is that Si_3N_4 has much lower phonon lifetimes and mean free paths (< 0.5 μm) due to the larger three-phonon scattering phase space and stronger anharmonicity. Interestingly, we find that the larger unit cell (with more basis atoms) that leads to a smaller fraction of acoustic phonons is not the reason for lower κ. Grain size-dependent κ indicates that the grain boundary scattering plays a negligible role

in most experimental samples. This work clarifies the theoretical κ upper limits of Si_3N_4 and can guide experimental research.

Keywords: Silicon nitride, thermal conductivity, first principles, phonons, thermal management

Thermal management of electronic devices plays a crucial role in normal operation where high temperature can degrade the performance and even destroy the devices, especially for highly integrated, high-power density, and miniaturized devices[1,2]. An excellent candidate material used for thermal management should have both high thermal conductivity and mechanical strength to prevent devices from overheating and fracture[3]. Silicon nitride (Si_3N_4) has received significant attention in this area owing to its superior properties. Because of the strong Si-N bond[4], Si_3N_4 ceramics exhibit excellent mechanical properties such as high strength at room and elevated temperatures and high hardness, which should lead to potential high thermal conductivity. Besides, Si_3N_4 possesses low thermal expansion, low density, and low dielectric constant[5–7]. All these outstanding properties qualify Si_3N_4 as a promising substrate candidate for high-power electronic devices.

There are three typical crystallographic structures of Si_3N_4, namely α-, β- and γ-Si_3N_4[8]. Among them, the γ phase is cubic, made through high temperature and high pressure, while the other two are more thermodynamically stable at room temperature with a hexagonal lattice[9]. β-Si_3N_4 is more stable at high temperatures and is the most commonly seen phase in applications. The α phase changes to β at high temperatures above 1300 °C[10]. While the mechanical properties of Si_3N_4 are guaranteed by the strong bonding, the thermal conductivities of α and β phase have not been well

studied yet. The theoretical study of the thermal conductivities of Si_3N_4 is very limited. In 1995, Haggerty and Lightfoot predicted the intrinsic thermal conductivity of β-Si_3N_4 to be 200 to 320 W/mK at room temperature based on Slack's relation[11]. In 2002, Hirosaki et al. revisited the theoretical values and predicted 170 and 450 W/mK along the *a* and *c* axes, respectively, by using molecular dynamics (MD) simulations with a classical potential[10]. They also reported the thermal conductivities of the α phase as 105 and 225 W/mK along the *a* and *c* axes, respectively. However, all these works were based on empirical models, which may cause large mispredictions. For example, Slack's relation has many fitting parameters, and the choice of those parameters is arbitrary. Classical potentials in MD simulations can give large errors for thermal conductivity as well. No first principles prediction has been carried out yet to unveil the intrinsic thermal conductivities of α- and β-Si_3N_4. Therefore, there is an urgency to accurately predict the theoretical upper limit of thermal conductivities to guide experimental efforts.

Driven by the literature's theoretical predictions, experiments have been continuously pursuing the upper limit of thermal conductivity of β-Si_3N_4, which is believed to be 200-450 W/mK, for more than two decades. In 1996, Hirosaki et al. obtained β-Si_3N_4 with a thermal conductivity of 120 W/mK by the addition of 1 mol% of Y_2O_3-Nd_2O_3 and sintering at 2000 °C[12]. They found that a higher sintering temperature can increase the thermal conductivity resulting from grain growth. In the same year, Hirao et al. reported a similar value of 122 W/mK for β-Si_3N_4 fabricated by tape casting[13]. Their samples exhibited a high anisotropy, which was attributed to the orientation of elongated grains. The thermal conductivity perpendicular to the stacking direction was measured to be around 60 W/mK. In 1999, Watari et al. increased the thermal conductivity of β-Si_3N_4 parallel to the casting direction to 155 W/mK by high-temperature firing and proper seeds

addition[14]. Though thermal conductivity along the other direction was still low, which was only 52 W/mK. In the same year, Li et al. enabled the measurement of a single β-Si_3N_4 grain and obtained 69 W/mK and 180 W/mK along the *a* and *c* axes, respectively[15]. They also indicated that anisotropy is intrinsic. Later, an isotropic thermal conductivity (149 W/mK) of β-Si_3N_4 was realized by Furuya et al. in 2002 by combining high-quality seed crystals with the suitable additive system to promote grain growth[16]. Afterward, β-Si_3N_4 produced by another method, namely, sintered reaction-bonding, which can provide lower cost and reduce the lattice oxygen was investigated by Zhu, Zhou, and coauthors[17–22] The highest thermal conductivity achieved was 177 W/mK. Moreover, many other experimental attempts have been made to promote the thermal conductivity of β-Si_3N_4 until today, and experimentalists assume the theoretical upper limit is 200-450 W/mK[23–31]. The reason the measured values have not reached this limit was believed to be the existence of the secondary phase (mainly lattice oxygen), grain boundary, and imperfections (vacancies, dislocations, etc.). However, it remains a question whether it is because the theoretical predictions are wrong.

In this letter, we unveil the intrinsic thermal conductivities of α- and β-Si_3N_4 by solving the phonon Boltzmann transport equation (BTE) based on first principles. The thermal conductivities of Si_3N_4 obtained are compared with literature data for Si_3N_4 and other promising ceramics. To understand the difference between them, we compare their phonon dispersions, velocities, lifetimes, and mean free paths (MFP). The impacts of grain size on thermal conductivities were also explored.

All the first principles calculations were performed by using the Vienna ab-initio simulation package (VASP)[32] with the projected augmented wave (PAW)[33] method based on the density functional theory (DFT). Local density approximation (LDA)[34] was chosen as the exchange-correlation functional. The plane-wave energy cutoff was selected as 500 eV. During the structure optimization process, atomic positions and the lattice constants were both allowed to be relaxed until the maximal residual energy was smaller than 10^{-8} eV. The force convergence threshold was 10^{-7} eV/Å. **K**-meshes of α- and β-Si_3N_4 are 6×6×9 and 8×8×16, respectively, to keep the consistency since different sizes of supercells were made in the force constant calculations. The obtained lattice constants for α-Si_3N_4 are 7.724 Å and 5.598 Å along *a* and *c* axes. For β-Si_3N_4, the lattice constants are 7.578 Å and 2.892 Å along *a* and *c* axes, respectively. All the results agree well with experimental data[35,36]. In the calculation of harmonic and anharmonic force constant using Phonopy[37] and Thirdorder[38], the supercell size was selected as 2×2×3 (336 atoms) with a 3×3×3 **k**-mesh for α-Si_3N_4 and 2×2×4 (224 atoms) with a 4×4×4 **k**-mesh for the β phase. The energy convergence threshold is 10^{-8} eV. The first principles calculation is computationally heavy due to the large unit cells. The non-analytical correction[39] that splits LO and TO phonons at Γ point was considered in the phonon dispersion calculations. Up to the 6th nearest neighbor of atoms were included for both phases in anharmonic force constant extraction. We do not consider four-phonon scattering since there is no acoustic-optical band gap, and we focus on low temperatures. The results compared to the experiment also indicate that four-phonon scattering is not important.

The temperature-dependent thermal conductivity, phonon MFP cumulative thermal conductivity, group velocity, scattering rate, and Grüneisen parameters were calculated by ShengBTE[38] using a

10×10×10 phonon **q**-mesh for α-Si_3N_4 and a 12×12×12 phonon **q**-mesh for β-Si_3N_4. The broadening factor was set to 0.1. The calculation convergence regarding **q**-mesh and broadening factor was tested. Natural isotope-phonon scattering was included. Grain size impact is included by using a phonon-boundary scattering rate τ_b^{-1} as [40]

$$\tau_{b,\lambda,i}^{-1} = \frac{2|v_{\lambda,i}|}{L} \quad (1)$$

where L is the grain size, b represents boundary, i indicates Cartesian directions, v is the group velocity, and λ represents a phonon mode with a certain wavevector and branch.

The phonon dispersions and densities of states of α- and β-Si_3N_4 are shown in Fig. 1. Both phases have high frequencies up to around 34 THz, indicating a strong bonding. Both phases have many atoms, i.e., 28 for α and 14 for β, in the primitive cell. As a result, the three acoustic phonon modes only occupy 3.57% and 7.14% of the total phonon modes for the α and β phases, respectively. Both phases have acoustic phonons up to around 7 THz, which was contributed by both Si and N atoms evenly based on the projected DOS.

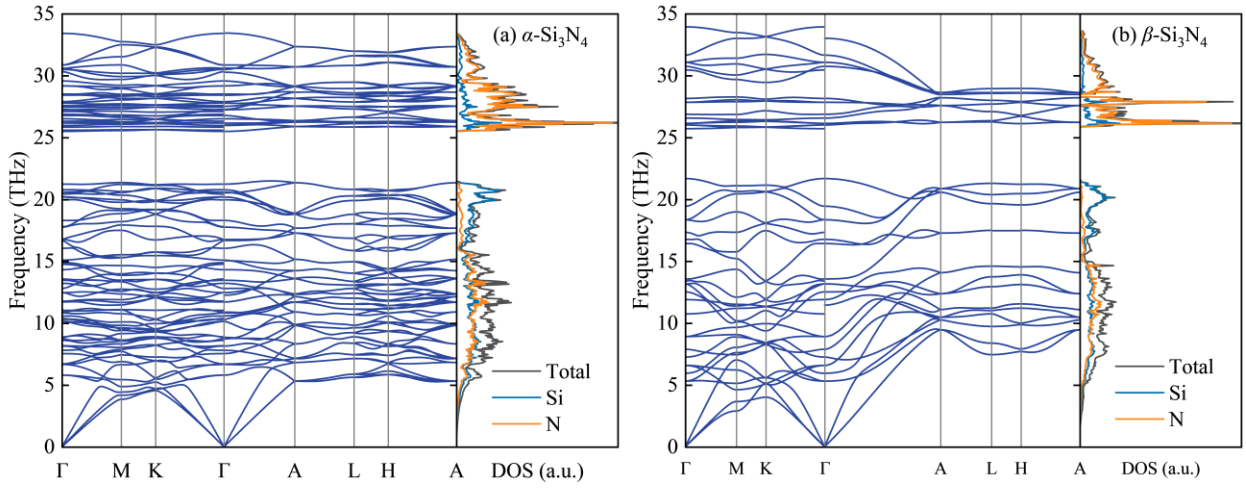

FIG.1. Phonon dispersions and densities of states (DOS) of (a) α-Si_3N_4 and (b) β-Si_3N_4.

The calculated temperature-dependent thermal conductivities of β-Si_3N_4 and corresponding experimental data from the literature are shown in Fig. 2 (a). The two curves represent our first principles results for the a and c axes, and the points are experimental data from the literature. Thermal conductivity along the *c* axis is larger than that along the *a* axis, which suggests an intrinsic anisotropy in the hexagonal lattice. Some of the experimental data reported the anisotropy of thermal conductivities, designated by squares and circles symbols with squares indicating the higher values[13–15,41,42], while the others only provided one single value without mentioning any details about the orientation-dependent information, designated by cross signs[12,16,18,22,25,28–30,43]. "//" and "⊥" indicate parallel or perpendicular to tape casting direction for Watari's[14] and Hirao's[13] results and hot-pressing direction for Kitayama's[41] and Liang's[42] results since they adopted different methods to produce Si_3N_4 samples. Based on our DFT calculations, the intrinsic thermal conductivities of β-Si_3N_4 at room temperature are 169 and 57 W/mK along the *c* and *a* axes, respectively, which are much smaller than Haggerty and Lightfoot's prediction based on Slack's relation[11] and Hirosaki's classical MD simulation[10]. This indicates that their estimations may mislead the audience.

As can be seen from the figure, at room temperature, almost all the experimental values are between our predicted thermal conductivities along two axes and some of them are very close to the intrinsic value along the *c* axis. For those experiments reporting anisotropic thermal conductivities along two perpendicular directions, some of them[14,15] reached our predicted value (upper limit) along the *c* axis, and the others did not[13,41]. Note that these experiments did not explicitly measure the a and c axes but two preferred perpendicular directions, which are not

necessarily aligned along the two axes. In other studies where there is only one single thermal conductivity reported, it can be understood as either the isotropic value due to disordered grains or just the thermal conductivity along a certain direction that is not specified. Based on our estimation, the upper and lower limit of isotropic thermal conductivities of β-Si_3N_4 are $(\kappa_a + \kappa_b + \kappa_c)/3 =$ 94.3 W/mK and $3/\left(\frac{1}{\kappa_a} + \frac{1}{\kappa_b} + \frac{1}{\kappa_c}\right) = 73.16\,\mathrm{W/mK}$, respectively. This means most of the values[18,22,25,28,30] reported should be along a certain direction since they are even larger than 100 W/mK. It should also be pointed out that the reported highest isotropic thermal conductivities (149 W/mK)[16] may not be reliable based on the above estimation. Among these experimental results, the highest one was achieved by Zhou *et al*.[22] in 2015 with a thermal conductivity of 177 W/mK, which is close to our prediction. The thermal conductivity reported by Li *et al.*[15] is slightly higher than Zhou *et al*.'s[22] value, but they just measured the thermal conductivity in a single grain instead of the whole material. Their in-grain intrinsic thermal conductivity value further validates our prediction.

Regarding the temperature dependent thermal conductivity, it can be seen from the figure that our predicted thermal conductivity agrees well with Watari *et al.*'s experimental data[14] throughout the whole temperature range, which is clear evidence that our prediction is accurate. If grain boundary or defects play a role in the experimental sample, its temperature dependence should be altered and be different from the $1/T$ trend predicted by first principles[44–47]. In addition, their perpendicular thermal conductivities are slightly larger than our simulated value along the *a* axis. This could be their reported value mistake since they reported 52 W/mK at room temperature but plotted as 68 W/mK in their figure. Note that 52 W/mK agrees with our prediction. We further checked the off-diagonal contribution since it can bend up the temperature-dependency trend of

thermal conductivity based on Wigner formulation[48]. However, it was found the contribution of off-diagonal term is only 0.5 W/mK at 1000 K, much smaller than the intrinsic value, which means it can be neglected. Moreover, it should be noted that DFT calculation cannot be absolutely accurate, since the use of different pseudopotentials, number of nearest neighbors, energy cutoff, etc. will all give slightly different results. However, considering the good agreement between the experimental efforts and our predictions, it can be concluded that our prediction of the thermal conductivity of β-Si_3N_4 is convincing and the experimental efforts have already reached the upper limit of the thermal conductivities of β-Si_3N_4. The hypothesis in the literature that the secondary phase (mainly lattice oxygen), grain boundary, and imperfections (vacancies, dislocations, etc.) degraded the thermal conductivity is likely not true. The existence of those factors should play insignificant role on the thermal conductivity of experimental samples.

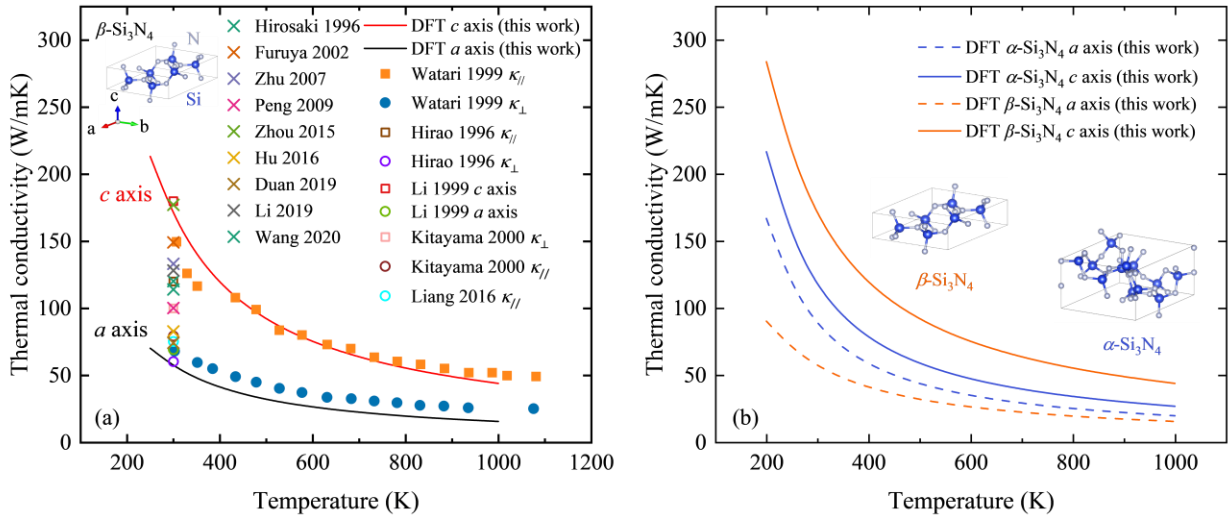

FIG. 2. (a) Temperature-dependent thermal conductivities of β-Si_3N_4 from first principles compared to experimental data from the literature; (b) Predicted temperature-dependent thermal conductivities of α-Si_3N_4 and β-Si_3N_4 from first principles.

Since the α phase is also commonly seen at room temperature, we have also predicted its thermal conductivity, as shown in Fig. 2 (b). Thermal conductivities of α-Si_3N_4 were found to be 87 and 116 W/mK along the *a* and *c* axes at room temperature, respectively. As the temperature goes up, thermal conductivities of both phases decrease. Overall, β-Si_3N_4 owns the highest thermal conductivity along the *c* axis but lowest along the *a* axis. α-Si_3N_4 shows less significant anisotropy compared with the β phase.

Since Si_3N_4 and SiC have similar Debye temperature, atomic bonding strength, mechanical strength, average atomic volume, and average atomic mass, based on Slack's relation, they should have comparable thermal conductivities[11]. Here, we compare the intrinsic thermal conductivities of Si_3N_4, 3C-SiC[49], 4H-SiC[50], 6H-SiC[50], AlN[51], and GaN[50], which are also promising semiconductors or substrates and have well-agreed thermal conductivities values from first principles prediction and experiment. As shown in Fig. 3, 3C-SiC possesses the highest thermal conductivity, which is 511 W/mK at room temperature. However, the intrinsic thermal conductivities of the three polymorphs of Si_3N_4 are much smaller than SiC and are the lowest among all the materials. This may suggest that Si_3N_4 may not be the best candidate for substrates in terms of thermal transport.

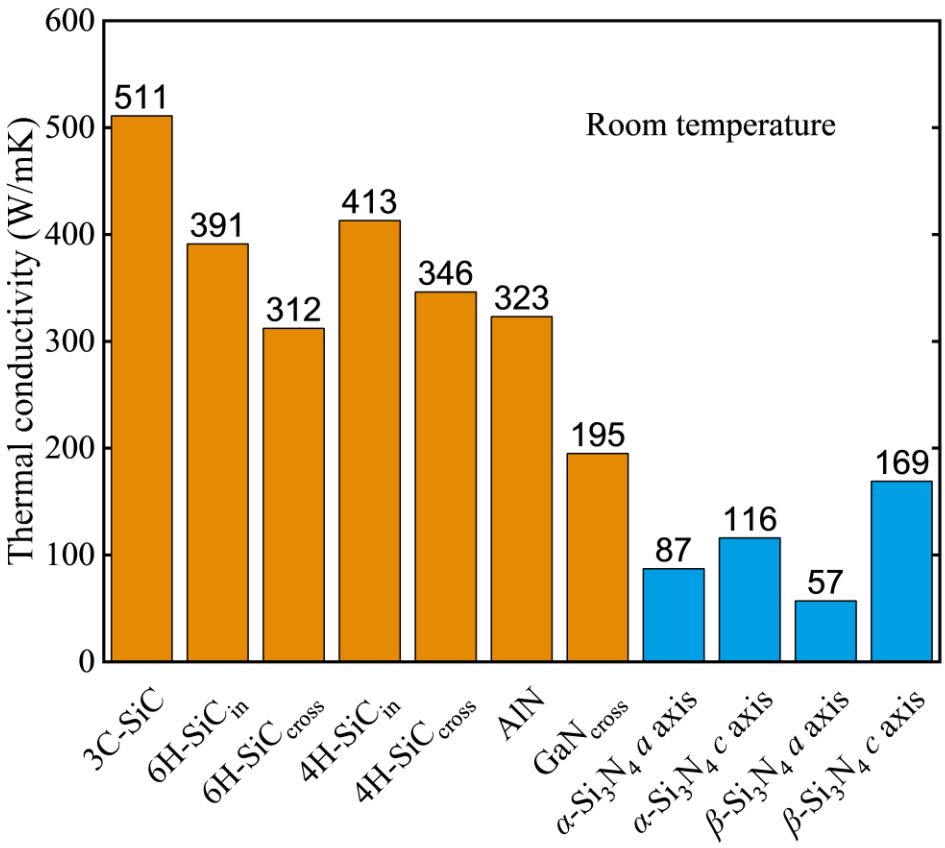

FIG. 3. Comparison of the thermal conductivities between Si_3N_4 and 3C-SiC[49], 6H-SiC[50], 4H-SiC[50], AlN[51], and GaN[50] at room temperature. AlN and GaN also have anisotropy but are not significant and not shown here.

To find out the reason why thermal conductivities of β-Si_3N_4 are much lower than other materials[49], we compare its phonon MFP-cumulative thermal conductivities, phonon group velocities, lifetimes, three-phonon scattering phase space, and Grüneisen parameters, with 3C-SiC at room temperature as shown in Fig. 4. We find that β-Si_3N_4 has much shorter MFP, slower group velocities, and shorter phonon lifetimes. For example, the medium MFP of β-Si_3N_4 along *a* and *c* axes are both around 80 nm, while that of 3C-SiC is 500 nm. The averaged group velocity of β-Si_3N_4 is much lower than that of 3C-SiC, even though they share the similar sound velocity

(phonon velocity at the low-frequency limit). The shorter lifetime of β-Si_3N_4 than 3C-SiC originates from the larger phonon-phonon scattering phase space and stronger anharmonicity as shown in Fig. 4 (d,e). However, it remains a question why the anharmonicity of Si_3N_4 is significant whiling having strong interatomic bonding. Firstly, the Young's modulus of Si_3N_4 (320 GPa[52]) is not as high as that of SiC (425 GPa[53]). This indicates the bond of Si_3N_4 is not as strong as that of SiC. Secondly, anharmonicity, although somewhat positively correlated to bonding strength, is not determined solely by bonding strength. The potential well can deviate from the parabolic shape in various ways, representing various forms of anharmonicity, even for the same spring constant (or strength of bonding).

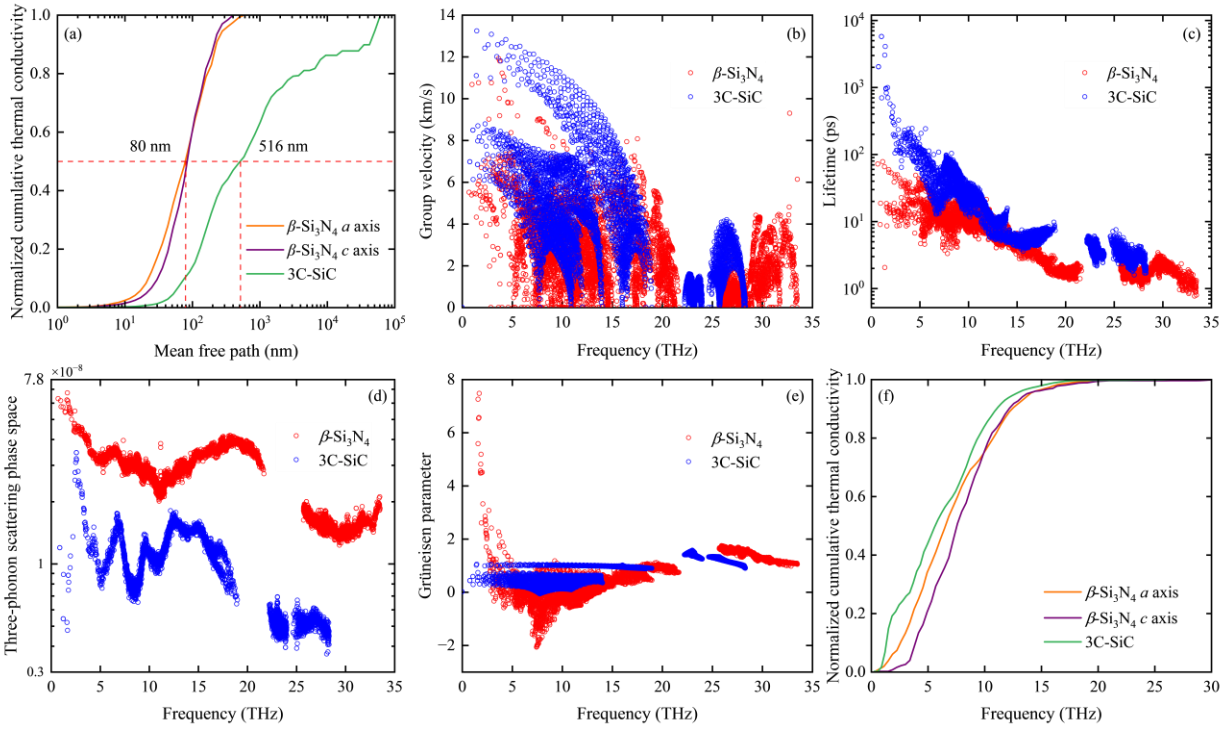

FIG. 4. Comparison between β-Si_3N_4 and 3C-SiC[49] at room temperature for (a) normalized MFP cumulative thermal conductivities, (b) phonon group velocities, (c) phonon lifetimes, (d) three-

phonon scattering phase space, (e) Grüneisen parameters, and (f) normalized frequency cumulative thermal conductivities.

It is usually believed that complex crystals have smaller thermal conductivity due to the smaller fraction of acoustic phonon modes, given the larger number of atoms in the unit cell. For example, the primitive cells of β-Si_3N_4 and 3C-SiC contain 14 and 2 atoms, respectively. As a result, the three acoustic modes only take 7.14% portion of the total number of phonon modes of Si_3N_4 but 50% of 3C-SiC. The acoustic phonon frequency range of Si_3N_4 is only 0-8 THz but is 0-19 THz for 3C-SiC[49]. However, after checking the frequency-cumulative thermal of the two materials conductivity as shown in Fig. 4 (f), a contradictory trend is found: the two materials have nearly identical frequency dependent thermal conductivity contribution. This finding shows that it is not true that optical phonons' contribution is not negligible and is comparable to acoustic phonons of Si_3N_4. Actually, the optical phonons contribute to 55.07% and 62.26 % of the thermal conductivity in Si_3N_4 along *a* and *c* axes. It indicates that the larger unit cell (with more basis atoms) that leads to smaller fraction of acoustic phonons is not the reason for lower thermal conductivity. This conclusion is in agreement with a recent study by Dai and Tian[54], who revealed that thermal conductivities of B_6O (i.e., α-B_6O and β-B_6O) could be as high as 200-300 W/mK even though they have complex crystal structures. It is also consistent with the fact that the different polytypes of a material have similar thermal conductivity even though their unit cell sizes differ by several times, for example thermal conductivities of SiC (i.e., 3C-SiC, 4H-SiC, 6H-SiC) are all around 400-500 W/mK. Here, the two polytypes of Si_3N_4 also have similar thermal conductivity of 80-90 W/mK (after averaging the anisotropy) even though their unit cell size differ significantly.

Since experimental samples often have grain boundaries, it is necessary to predict the impact of grain sizes on thermal transport. As shown in Fig. 5, the thermal conductivity of a grain can reaches 80% of bulk thermal conductivity at the size of 0.4 μm for the *a* axis, and 90% at the size of 0.6 μm for the *c* axis. It is safe to conclude that once the grain size is larger than 2 μm, grain size plays a little role in the measured thermal conductivities. Since the grain size of most of the experimental samples is large enough[15,22,23,27], the impact of grain size should not be a concern in the experiments.

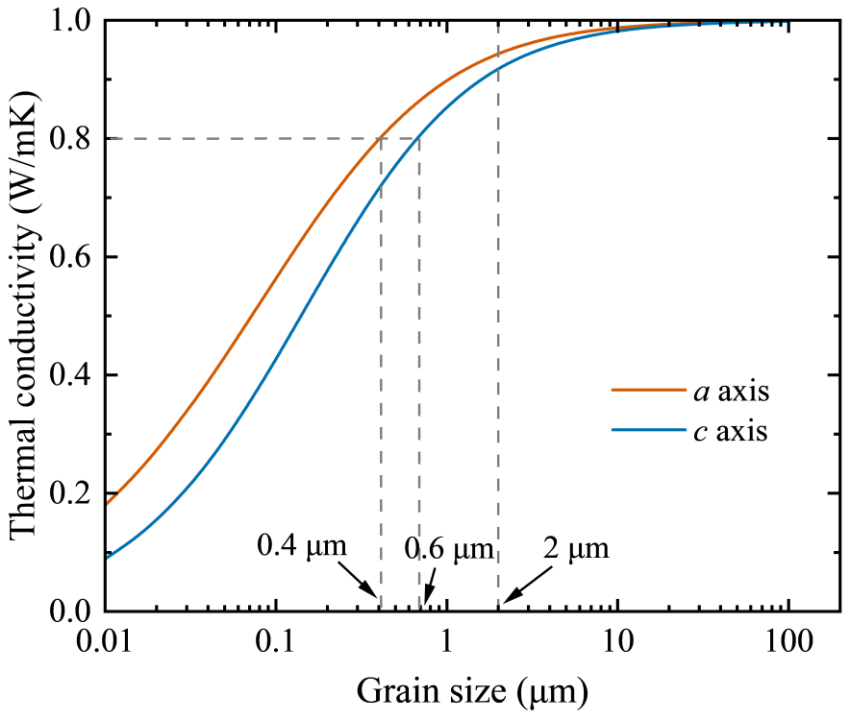

FIG. 5. Normalized grain size dependent thermal conductivity of β-Si_3N_4 along *a* and *c* axes.

To summarize, we have revisited the theoretical thermal conductivity upper limit of α- and β-Si_3N_4 by using first principles. We find that they are much smaller than believed. The thermal conductivities of β-Si_3N_4 at room temperature are 169 and 57 W/mK along the *c* and *a* axes, respectively. For the α phase, they are 116 and 87 W/mK. The previous high predictions based on

empirical models are not reliable. The experimental efforts in the literature have already reached the upper limit of the β-Si_3N_4. The large volume for three-phonon scattering and anharmonicity of β-Si_3N_4 are responsible for the lower thermal conductivity of Si_3N_4 compared to other similar ceramics such as SiC, AlN, and GaN. Grain size-dependent thermal conductivity results suggest that the impact of grain size is negligible in most experiments as their grains are usually larger than 2 μm. We expect this work to be crucial in semiconductors development.

References

[1] H. Okumura, Jpn J Appl Phys **45**(10R), 7565 (2006).

[2] S.P. Gurrum, S.K. Suman, Y.K. Joshi, and A.G. Fedorov, IEEE Transactions on Device and Materials Reliability **4**(4), 709–714 (2004).

[3] D. Graovac, A. Christmann, and M. Munzer, in *8th International Conference on Power Electronics - ECCE Asia* (IEEE, 2011), pp. 1666–1673.

[4] F. Gao, J. He, E. Wu, S. Liu, D. Yu, D. Li, S. Zhang, and Y. Tian, Phys Rev Lett **91**(1), 015502 (2003).

[5] R.N. Katz, MRS Proceedings **287**, 197 (1992).

[6] F.L. Riley, Journal of the American Ceramic Society **83**(2), 245–265 (2000).

[7] H. Klemm, Journal of the American Ceramic Society **93**(6), 1501–1522 (2010).

[8] A. Kuwabara, K. Matsunaga, and I. Tanaka, Phys Rev B Condens Matter Mater Phys **78**(6), 1–11 (2008).

[9] J. Liu, S. Ju, N. Nishiyama, and S. Junichiro, Phys Rev B **100**(6), 064303 (2019).

[10] N. Hirosaki, S. Ogata, C. Kocer, H. Kitagawa, and Y. Nakamura, Phys Rev B **65**(13), 134110 (2002).

[11] J.S. Haggerty, and A. Lightfoot, in *Ceramic Engineering & Science Proceedings* (1995), p. 475.

[12] N. Hirosaki, Y. Okamoto, M. Ando, F. Munakata, and Y. Akimune, Journal of the American Ceramic Society **79**(11), 2878–2882 (1996).

[13] K. Hirao, K. Watari, M.E. Brito, M. Toriyama, and S. Kanzak, Journal of the American Ceramic Society **79**(9), 2485–2488 (1996).

[14] K. Watari, K. Hirao, M.E. Brito, M. Toriyama, and S. Kanzaki, J Mater Res **14**(4), 1538–1541 (1999).

[15] B. Li, L. Pottier, J.P. Roger, D. Fournier, K. Watari, and K. Hirao, J Eur Ceram Soc **19**(8), 1631–1639 (1999).

[16] K. Furuya, F. Munakata, K. Matsuo, Y. Akimune, J. Ye, and A. Okada, J Therm Anal Calorim **69**(3), 873–879 (2002).

[17] X. Zhu, Y. Zhou, K. Hirao, and Z. Lenčéš, Journal of the American Ceramic Society **89**(11), 3331–3339 (2006).

[18] X. Zhu, Y. Zhou, K. Hirao, and Z. Lenčéš, Journal of the American Ceramic Society **90**(6), 1684–1692 (2007).

[19] Y. Zhou, X. Zhu, K. Hirao, and Z. Lences, Int J Appl Ceram Technol **5**(2), 119–126 (2008).

[20] X.W. Zhu, Y. Sakka, Y. Zhou, and K. Hirao, Journal of the Ceramic Society of Japan **116**(1354), 706–711 (2008).

[21] Y. Zhou, H. Hyuga, D. Kusano, Y.I. Yoshizawa, and K. Hirao, Advanced Materials **23**(39), 4563–4567 (2011).

[22] Y. Zhou, H. Hyuga, D. Kusano, Y. ichi Yoshizawa, T. Ohji, and K. Hirao, Journal of Asian Ceramic Societies **3**(3), 221–229 (2015).

[23] W. Wang, D. Yao, H. Liang, Y. Xia, K. Zuo, J. Yin, and Y.P. Zeng, J Eur Ceram Soc **41**(2), 1735–1738 (2021).

[24] Y. Wang, X. Li, H. Wu, B. Jia, D. Zhang, Y. Zhang, Z. Zhang, J. Tian, M.L. Qin, and X. Qu, Unpublished, (2021).

[25] W. Wang, D. Yao, H. Chen, Y. Xia, K. Zuo, J. Yin, H. Liang, and Y. Zeng, Journal of the American Ceramic Society **103**(3), 2090–2100 (2020).

[26] F. Hu, Z.P. Xie, J. Zhang, Z.L. Hu, and D. An, Rare Metals **39**(5), 463–478 (2020).

[27] H. Liang, W. Wang, K. Zuo, Y. Xia, D. Yao, J. Yin, and Y. Zeng, Ceram Int **46**(11), 17776–17783 (2020).

[28] Y. Li, H.N. Kim, H. Wu, M.J. Kim, J.W. Ko, Y.J. Park, Z. Huang, and H.D. Kim, J Eur Ceram Soc **39**(2–3), 157–164 (2019).

[29] F. Hu, L. Zhao, and Z.P. Xie, Journal of Ceramic Science and Technology **7**(4), 423–428 (2016).

[30] G.H. Peng, M. Liang, Z.H. Liang, Q.Y. Li, W.L. Li, and Q. Liu, Journal of the American Ceramic Society **92**(9), 2122–2124 (2009).

[31] S. LIAO, L. ZHOU, K. YIN, J. WANG, and C. JIANG, Materials Reports **34**(11), 21105–21114 (2020).

[32] G. Kresse, and J. Furthmüller, Phys Rev B **54**(16), 11169–11186 (1996).

[33] P.E. Blöchl, Phys Rev B **50**(24), 17953–17979 (1994).

[34] J.P. Perdew, and A. Zunger, Phys Rev B **23**(10), 5048–5079 (1981).

[35] D. du Boulay, N. Ishizawa, T. Atake, V. Streltsov, K. Furuya, and F. Munakata, Acta Crystallogr B **60**(4), 388–405 (2004).

[36] H. Toraya, J Appl Crystallogr **33**(1), 95–102 (2000).

[37] A. Togo, F. Oba, and I. Tanaka, Phys Rev B **78**(13), 134106 (2008).

[38] W. Li, J. Carrete, N. A. Katcho, and N. Mingo, Comput Phys Commun **185**(6), 1747–1758 (2014).

[39] K. Parlinski, Z.Q. Li, and Y. Kawazoe, Phys Rev Lett **78**(21), 4063–4066 (1997).

[40] A.J.H. McGaughey, E.S. Landry, D.P. Sellan, and C.H. Amon, Appl Phys Lett **99**(13), 131904 (2011).

[41] M. Kitayama, K. Hirao, A. Tsuge, K. Watari, M. Toriyama, and S. Kanzaki, Journal of the American Ceramic Society **83**(8), 1985–1992 (2000).

[42] H. Liang, Y. Zeng, K. Zuo, Y. Xia, D. Yao, and J. Yin, Ceram Int **42**(14), 15679–15686 (2016).

[43] Y. Duan, J. Zhang, X. Li, H. Bai, P. Sajgalik, and D. Jiang, Int J Appl Ceram Technol **16**(4), 1399–1406 (2019).

[44] J.S. Kang, M. Li, H. Wu, H. Nguyen, and Y. Hu, Science (1979) **361**(6402), 575–578 (2018).

[45] S. Li, Q. Zheng, Y. Lv, X. Liu, X. Wang, P.Y. Huang, D.G. Cahill, and B. Lv, Science (1979) **361**(6402), 579–581 (2018).

[46] F. Tian, B. Song, X. Chen, N.K. Ravichandran, Y. Lv, K. Chen, S. Sullivan, J. Kim, Y. Zhou, T.H. Liu, M. Goni, Z. Ding, J. Sun, G.A.G.U. Gamage, H. Sun, H. Ziyaee, S. Huyan, L. Deng, J. Zhou, A.J. Schmidt, S. Chen, C.W. Chu, P.Y. Huang, D. Broido, L. Shi, G. Chen, and Z. Ren, Science (1979) **361**(6402), 582–585 (2018).

[47] T. Feng, A. O'Hara, and S.T. Pantelides, Nano Energy **75**, 104916 (2020).

[48] M. Simoncelli, N. Marzari, and F. Mauri, Phys Rev X **12**(4), 1–34 (2022).

[49] Z. Cheng, J. Liang, K. Kawamura, H. Zhou, H. Asamura, H. Uratani, J. Tiwari, S. Graham, Y. Ohno, Y. Nagai, T. Feng, N. Shigekawa, and D.G. Cahill, Nat Commun **13**(1), 7201 (2022).

[50] Q. Zheng, C. Li, A. Rai, J.H. Leach, D.A. Broido, and D.G. Cahill, Phys Rev Mater **3**(1), 014601 (2019).

[51] Z. Cheng, Y.R. Koh, A. Mamun, J. Shi, T. Bai, K. Huynh, L. Yates, Z. Liu, R. Li, E. Lee, M.E. Liao, Y. Wang, H.M. Yu, M. Kushimoto, T. Luo, M.S. Goorsky, P.E. Hopkins, H. Amano, A. Khan, and S. Graham, Phys Rev Mater **4**(4), 044602 (2020).

[52] R.J. Bruls, H.T. Hintzen, G. de With, and R. Metselaar, J Eur Ceram Soc **21**(3), 263–268 (2001).

[53] R. Anzalone, M. Camarda, A. Canino, N. Piluso, F. La Via, and D. D'Arrigo, Electrochemical and Solid-State Letters **14**(4), H161 (2011).

[54] J. Dai, and Z. Tian, Appl Phys Lett **118**(4), (2021).

Data availability

Source data are provided with this paper. All other data that support the plots within this paper are available from the corresponding authors on reasonable request.

Code availability

The codes used in this study are available from the corresponding authors upon request.

Acknowledgments

This work is supported by the National Science Foundation (NSF) (award number: CBET 2212830). The computation used the resources from the Center for High Performance Computing (CHPC) at the University of Utah, the Advanced Cyberinfrastructure Coordination Ecosystem: Services & Support (ACCESS) of NSF, and the National Energy Research Scientific Computing Center (NERSC), a DOE Office of Science User Facility under Contract No. DE-AC02-05CH11231 and award No. BES-ERCAP0022132.

Author contributions

T.F. conceived the idea and guided the project. H.Z. performed the simulations and wrote the original manuscript. H.Z. and T.F. both revised the manuscript.

Competing interests

The authors declare no competing interests.

Additional information

Correspondence and requests for materials should be addressed to T.F.